CRYSTAL GROWTH & DESIGN

Article

Cite This: Cryst. Growth Des. 2019, 19, 2089−2096

pubs.acs.org/crystal

Electrospray Mass Spectrometry Investigation into the Formation of CPO-27

Mali H. Rosnes,*[,†] Jennifer S. Mathieson,[‡] Karl W. Törnroos,[†] Rune E. Johnsen,[§] Leroy Cronin,[‡] and Pascal D. C. Dietzel*[,†]

[†]Department of Chemistry, University of Bergen. P.O. Box 7803, 5020 Bergen, Norway

[‡]School of Chemistry, WestCHEM, University of Glasgow, Glasgow G12 8QQ, Scotland

[§]Department of Energy Conversion and Storage Technical University of Denmark, Frederiksborgvej 399, 4000 Roskilde, Denmark

Supporting Information

ABSTRACT: Electrospray ionization mass spectrometry (ESI-MS) has been utilized to investigate the self-assembly processes occurring during the formation of the microporous metal−organic framework CPO-27-M (M = Co, Ni). The mono- and dinuclear building units {M($H_x$dhtp)} and {M_2($H_x$dhtp)}, where $H_x$dhtp is the organic linker $H_xC_8O_6$ and fragments thereof, were identified as key species present in the reaction mixture during the product formation. Time-resolved powder X-ray diffraction analysis was used to follow the synthesis and confirmed that no other crystalline products occur in the reaction mixture prior to the crystallization of CPO-27-Ni. When equimolar reactions were performed at room temperature, compounds [(M(H_2dhtp)(H_2O)$_4$·2H_2O] (M = Co, Ni) crystallized instead of CPO-27 obtained at the higher temperature of the solvothermal procedure. It was confirmed that mono- and dinuclear species are key building blocks not only in the formation of CPO-27-M but also in the formation of the 1D chain structure (M(H_2dhtp)(H_2O)$_4$) obtained from these room-temperature reactions.

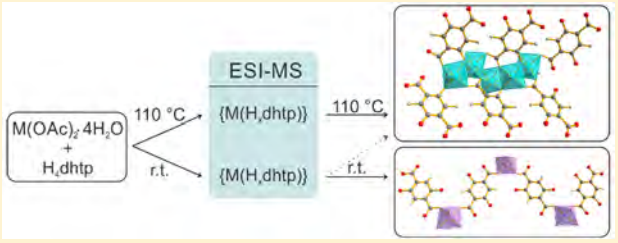

INTRODUCTION

Metal−organic frameworks (MOFs), also known as porous coordination polymers (PCPs), have attracted a great deal of attention due to their crystalline, often porous, structures, associated with high specific surface areas. Permanently porous MOFs have been intensely studied over the last few decades, with great promise for a diverse number of application areas.[1−3] However, while a coherent understanding of the crystallization process is of significant interest for the improved development of materials, studies of how these solids self-assemble in solution are scarce.

Over the last few decades mass spectrometry (MS) has gained vast interest as a technique to investigate self-assembly processes, to study solution species, and to follow reactions over time in order to gain an understanding of how reactions proceed, along with aiding in structure determination.[4,5] Electrospray ionization mass spectrometry (ESI-MS) has been used to investigate materials from silver coordination polymers to the self-assembly of metallodendrimers.[6,7] It has also been used to confirm the structure of complex compounds and to investigate the self-assembly process in materials such as polyoxometalates (POMs).[8−10] ESI-MS has been predicted to be a key tool in the further understanding of MOF formation.[11]

Whereas POMs are discrete nanosized metal−oxide polyanions, MOFs are infinite hybrid networks. This results in behaviors very different from what is typically observed for POMs, such as poorer solubility, which makes it more challenging to carry out ESI-MS investigations of MOFs. A workaround for this problem was reported by Garibay et al., where they digested the MOFs and used ESI-MS to identify and confirm the presence of multiple functional groups.[12] There are also a few examples highlighting the potential of using ESI-MS and cryospray (temperature-controlled) electrospray mass spectrometry (CSI-MS) to investigate the self-assembly processes occurring during the formation of zeolites and MOFs.[11,13−19]

Herein, we investigate the well-known isostructural series CPO-27-M, also denoted M_2(dhtp), M_2(dobdc) (dhtp/dobdc^{4-} = $C_8H_2O_6^{4-}$ (2,5-dioxidoterephthalate)), or M-MOF-74, where M = Co,[20] Ni.[21] The structure is also formed with other divalent cations such as M = Mg,[22] Mn,[23] Zn,[24] Fe,[25,26] Cu,[27−29] Cd.[30] The CPO-27 series consists of a honeycomb-like structure with hexagonal pores roughly 1.2 nm in diameter. The chain composing the inorganic secondary building unit of the CPO-27-M structure is shown at the top of Figure 1. The CPO-27-M series has been intensely studied due to its interesting structure, which contains an extraordinarily high concentration of open metal sites, and has potential in applications related to high storage capacity at lower pressures

Received: November 5, 2018
Revised: February 26, 2019
Published: February 28, 2019

DOI: 10.1021/acs.cgd.8b01657
Cryst. Growth Des. 2019, 19, 2089−2096

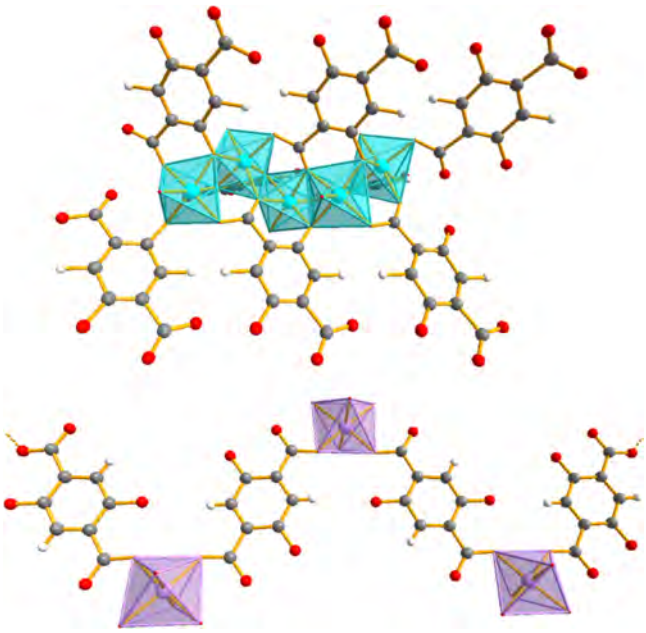

Figure 1. (Top) Structure excerpt emphasizing the inorganic secondary building unit of CPO-27-Ni, where all oxygen atoms of the $dhtp^{4-}$ units are coordinated to nickel atoms so that a helical chain of condensed metal oxygen octahedra is formed. (Bottom) 1D chain structure of $[(M(H_2dhtp)(H_2O)_4{\cdot}2H_2O]$ (M = Co, Ni), containing isolated metal oxygen octahedra. Nickel is shown in teal, cobalt in purple, carbon in gray, oxygen in red, and hydrogen on benzene rings in white. The remaining hydrogen atoms, rotational disorder of benzene rings, and noncoordinated water molecules are omitted for clarity.

and high selectivity in gas sorption from gas mixtures.[31,32] For instance, the compounds in the CPO-27-M series have been found to have exceptionally good CO_2 adsorption properties, with CPO-27-Mg at 0.1 atm reported to have the highest CO_2 capacity of all MOFs.[33,34] However, the adsorption properties of the CPO-27-M compounds in general, and CPO-27-Mg in particular, are negatively affected under humid conditions.[35]

A key to successfully realize the potential associated with MOFs lies in understanding their self-assembly process.[36] Typically the syntheses of MOFs are carried out under solvothermal conditions.[37−39] One of the reasons the assembly of MOFs is not fully understood is due to the difficulties associated with directly analyzing reaction mixtures in the experimental setups usually used to prepare MOFs and due to the many parameters, such as temperature, pressure, reactant concentration, and solvent system, that affect the synthetic conditions. However, a number of studies are available which discuss the crystallization processes involved, usually using diffraction techniques,[40−44] as well as a range of other techniques.[14] However, it is challenging to establish a link between solid-state and solution-based self-assembly. The formation of materials typically occurs via hydrolysis or condensation,[36,45] with ligand exchange reactions playing a key role.

Herein, we investigate the synthesis of CPO-27-Ni and -Co by ESI-MS. The two members of the series were chosen because they can both be synthesized by employing the same synthetic procedure, using THF and H_2O as solvent, which is compatible with the requirements for the experimental conditions of the ESI-MS technique. Nickel-containing species are easily identified in MS spectra due to their well-defined isotopic contribution to the MS peak envelopes. This significantly aids in the identification of the species in the spectra. Cobalt, on the other hand, does not have such a distinct isotope pattern, but a comparison of peaks between Ni and Co spectra can be used to confirm the peak assignments.

EXPERIMENTAL DETAILS

Instrumentation. *Low-Resolution ESI-MS.* The instrument used was an Agilent 6420A triple-quadrupole (QqQ configuration) mass analyzer using electrospray ionization (ESI). It was connected to an Agilent 1200 series LC module (binary pump, column compartment/oven, and autosampler). The eluent stream was introduced directly into the source, at a dry gas temperature of 200 °C. The ion polarity for all MS scans recorded was positive, with the voltage of the capillary tip set at 3500 V. The scan time was 500 ms, and the cell accelerator voltage was 7 V. The fragmentor was set at 120 and 175 V for the starting materials and at 175 V for the reaction mixtures. Initial experiments were also carried out in negative mode ESI-MS; however, species from H_4dhtp dominate these spectra, and no additional information regarding the speciation of H_4dhtp with metal acetate was obtained. As a consequence, we report only positive mode ESI-MS. Aliquots used for ESI-MS injections were diluted with MeOH or 1:9 (v:v) H_2O and MeOH mixtures (to avoid formation of precipitate) to reach concentrations compatible with the MS (about 1×10^{-2} to 1×10^{-3} mol L^{-1} with respect to the original transition-metal concentration).

High-Resolution ESI-MS. The MS apparatus used was a Bruker MaXis Impact instrument, calibrated using an Agilent ESI-L tuning mix for the mass range m/z 100−3000. The eluent stream was introduced directly into the source, at a dry gas temperature of 200 °C. The ion polarity for all MS scans recorded was positive, with the voltage of the capillary tip set at 4800 V, end plate offset at −500 V, funnel 1 radio frequency (rf) at 400 Vpp and funnel 2 rf at 400 Vpp, hexapole rf at 100 Vpp, ion energy 5.0 eV, collision energy at 5 eV, collision cell rf at 200 Vpp, transfer time at 100.0 μs, and prepulse storage time at 1.0 μs. Aliquots used for ESI-MS injections were diluted with MeOH or 1:9 (v:v) H_2O and MeOH mixtures (to avoid any precipitate formation) to reach MS-compatible concentrations (about 1×10^{-4} to 1×10^{-5} mol L^{-1} with respect to the original transition-metal concentration taking into account the sensitivity of the instrument).

Powder X-ray Diffraction. PXRD measurements were carried out on a Bruker AXS D8 Advance diffractometer equipped with a nine-position sample changer. Data collection was performed using monochromatic Cu Kα_1 radiation in Bragg−Brentano geometry.

Single-Crystal X-ray Diffraction. Suitable as-synthesized single crystals for diffraction experiments were mounted under ambient conditions in a minimum amount of Parabar 10312 oil (Hampton Research) in nylon loops. Intensity data were collected with a Bruker AXS TXS rotating anode system with an APEXII Pt^{135} CCD detector using graphite-monochromated Mo Kα radiation (λ = 0.71073 Å). The CCDC 1499898 reference code contains supplementary crystallographic data for this paper. The data can be obtained free of charge from The Cambridge Crystallographic Data Centre via www.ccdc.cam.ac.uk/data_request/cif.

Synchrotron Experiments. The X-ray diffraction experiment was performed at the Swiss-Norwegian Beamline (BM01A) at ERSF. A hot-air blower was programmed to heat the capillary containing the solution from room temperature to 110 °C with a heating gradient of 5 °C min^{-1}. Diffraction data were collected during the heating using a MAR345 area detector. A wavelength of 0.7207 Å, a sample to detector distance of 300 mm with a slit size of 0.5 × 0.5 mm, and an exposure time of 20 s were used. This resulted in a time resolution of 107.2 s per pattern (exposure time plus data readout time). The data were converted to normal one-dimensional powder pattern using the program FIT2D.[46]

Materials. All chemicals, reagents, and solvents were purchased from Sigma-Aldrich and used as received without further purification.

DOI: 10.1021/acs.cgd.8b01657
Cryst. Growth Des. 2019, 19, 2089−2096

Synthetic Methods. *Reactions Carried Out at 110 °C. 2:1 Ratio of $M(OAc)_2{\cdot}4H_2O$ (M = Co, Ni) and 2,5-Dihydroxyterepthalic Acid (H_4dhtp).* Either cobalt or nickel acetate tetrahydrate (0.207 g, 0.833 mmol) was dissolved in 5 mL of H_2O and H_4dhtp (0.083 g, 0.417 mmol) in 5 mL of THF, before the reagents were mixed in a 23 mL Teflon insert. After the mixture was stirred for 5 min the initial MS sample was taken, before the Teflon inserts were sealed in steel autoclaves and put in the oven at 110 °C. Several parallel reactions were set up simultaneously and stopped at different time intervals, from 30 min to 24 h. The steel autoclaves were cooled to room temperature before they were opened, and a sample for MS analysis was extracted by a micropipette. The solid products were obtained by filtration and washed with H_2O. For stock solutions, larger scale of the reported procedure was prepared.

1:1 Ratio of $M(OAc)_2{\cdot}4H_2O$ (M = Co, Ni) and H_4dhtp. Either cobalt or nickel acetate tetrahydrate (0.207 g, 0.833 mmol) was dissolved in 5 mL of H_2O and the H_4dhtp (0.165 g, 0.833 mmol) in 5 mL of THF, before the reagents were mixed in a 23 mL Teflon insert. After the mixture was stirred for 5 min, the initial MS sample was taken, before the Teflon inserts were sealed in steel autoclaves and put in the oven at 110 °C. Several parallel reactions were set up simultaneously and stopped at different time intervals, from 30 min to 24 h. The steel autoclaves were cooled to room temperature before they were opened, and a sample for MS analysis were extracted by a micropipette. The solid products were obtained by filtration and washed with H_2O. For stock solutions, larger scale of the reported procedure was prepared.

Reactions Carried Out at Room Temperature. These reactions were performed in glass vials, and the starting concentration of each of the reagents was kept constant. For all reactions the reagents were mixed in a glass vial and stirred for 5 min before the initial MS sample was taken and the vial sealed and left undisturbed. After about 48 h a precipitate started forming. The products were collected by filtration and washed with H_2O.

2:1 Ratio of $M(OAc)_2{\cdot}4H_2O$ (M = Co, Ni) and H_4dhtp. A solution of either cobalt or nickel acetate tetrahydrate in H_2O (0.167 mol L^{-1}) and a solution of H_4dhtp in THF (0.083 mol L^{-1}) were combined with a v/v ratio of 1.

1:1 Ratio of $M(OAc)_2{\cdot}4H_2O$ (M = Co, Ni) and H_4dhtp. A solution of either cobalt or nickel acetate tetrahydrate in H_2O (0.167 mol L^{-1}) and a solution of H_4dhtp in THF (0.167 mol L^{-1}) were combined with a v/v ratio of 1.

Experimental Details for Time-Resolved PXRD Experiment. A solution of $Ni(OAc)_2{\cdot}4H_2O$ (3×10^{-4} mol) in 1 mL of water and a solution of 2,5-dihydroxyterephthalic acid (1.5×10^{-4} mol) in 1 mL of THF were prepared. Equal volumes of each solution were combined into a 0.5 mm glass capillary. The capillary was flame-sealed, resulting in approximately equal volumes of liquid and gas phase, which correspond to the conditions under the standard solvothermal synthesis of CPO-27-Ni.[18] The capillary was glued onto the tip of a goniometer head. The diffraction experiment commenced approximately 30 min after mixing the solutions.

RESULTS

In this work, we investigate the MS results of the reaction mixtures before, during, and after the formation of CPO-27-Ni and -Co. First, we describe the MS analysis results of the starting materials and, second, of the initial reaction mixtures (before any solid product is observed). Third, we follow the reactions at room temperature and at 110 °C by ESI-MS, both before and during solid product formation. Finally, we relate the results of the ESI-MS and the synchrotron experiments.

Both CPO-27-Ni and -Co can be made using either 1:1 or 2:1 mixtures of $M(OAc)_2{\cdot}4H_2O$ (M = Co, Ni) and 2,5-dihydroxytherephthalic acid (H_4dhtp), and both reaction setups are discussed herein. The solvent mixture used was a 1:1 (v:v) mixture of H_2O and THF. Aliquots used for ESI-MS injections were diluted with MeOH or 1:9 (v:v) H_2O and MeOH mixtures to reach MS-compatible concentrations. The starting materials were extensively investigated by ESI-MS in advance to create a complete library of the species forming in solution in the absence of the reaction partner. Figure 2 shows a typical mass spectrum of $Ni(OAc)_2{\cdot}4H_2O$ and H_4dhtp. The equivalent for $Co(OAc)_2{\cdot}4H_2O$ and the corresponding assignments are shown in Section S2.1 in the Supporting Information (SI). An overview of when different aliquots were taken is shown in Scheme S1 in the Supporting Information. For reactions at 110 °C multiple reactions from the same stock solutions were setup in parallel and stopped at different time intervals to obtain information about the evolution of the MS spectra with time.

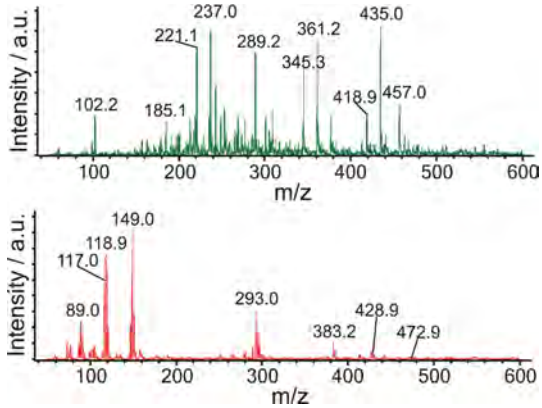

Figure 2. Typical MS spectra of H_4dhtp (top) and $Ni(OAc)_2{\cdot}4H_2O$ (bottom). See SI for further information. See Figure S2 for $Co(OAc)_2{\cdot}4H_2O$. The assignments are given in Table S2. The result for H_4dhtp is shown in Table S1. The species at m/z 118.9 is assigned to $[Na(CH_3OH)_3]^+$.

Investigations into the Initial Mixtures. $M(OAc)_2{\cdot}4H_2O$ and H_4dhtp were dissolved in H_2O and THF, respectively, before they were mixed and stirred for less than 5 min. No formation of solid product was observed at this point. An aliquot used for ESI-MS injections was diluted with MeOH or a 1:9 (v:v) H_2O and MeOH mixture to reach MS-compatible concentrations before being subjected to ESI-MS analysis.

New species are formed within the first 1 min after the two starting materials are mixed (which is the fastest time scale we can measure on), as can be seen in the mass spectrum of the $Ni(OAc)_2{\cdot}4H_2O$ and H_4dhtp mixture, shown in Figure 3, in

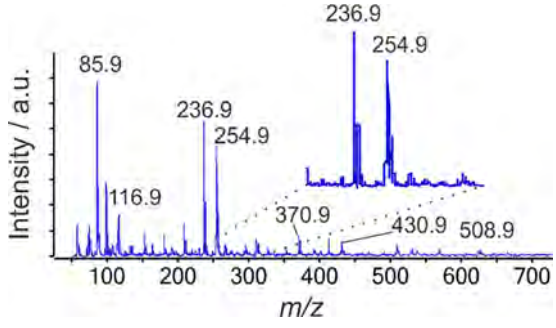

Figure 3. Example of a typical MS spectrum of the initial 1:1 molar ratio mixture of $Ni(OAc)_2$ and H_4dhtp. The species found at m/z 236.9 has been assigned to $[Ni(C_8H_3O_5)]^+$.

DOI: 10.1021/acs.cgd.8b01657
Cryst. Growth Des. 2019, 19, 2089−2096

comparison with the individual starting materials in solution, shown in Figure 2. Assignments of the main species observed for both the Co and Ni reactions are given in Table 1. Several species are identifiable as belonging to the solvent and the starting materials below m/z 150, but new species are also observed at higher m/z. The most evident are m/z 236.9/237.9 and 254.9/255.9, both assigned to $\{M(H_xdhtp)\}$ species (where H_xdhtp represents $H_xC_8O_6$ and fragments thereof); see Table 1 for further details. The second most evident and intense species are observed at m/z 370.9/372.9 and 430.9/432.9, both assigned to $\{M_2(H_xdhtp)\}$ species. For the Co reactions m/z 432.9, assigned to $\{M_2(H_xdhtp)\}$, is sometimes almost equal in intensity to m/z 255.9. This is followed (in intensity) by species of typically significantly lower intensity assigned to $\{M_2(H_xdhtp)_2\}$, $\{M_3(H_xdhtp)_2\}$, and $\{M_3(H_xdhtp)_3\}$ complexes with solvent and/or acetate adducts.

Table 1. Most Prominent Species in the Low-Resolution ESI-MS of the Initial 1:1 Mixture of $Ni(OAc)_2{\cdot}4H_2O$ with H_4dhtp (Left) and $Co(OAc)_2{\cdot}4H_2O$ with H_4dhtp (Right)

m/z (M = Ni)	assignment[a]	m/z (M = Co)
236.9	$[M(C_8H_3O_5)]^+$	237.9
254.9	$[M(C_8H_5O_6)]^+$	255.9
286.9	$[M(C_8H_5O_6)(CH_3OH)]^+$	287.9
292.8	$[M_2(CH_3COO)_3]^+$	294.9
370.9	$[M_2(C_8H_4O_6)(CH_3COO)]^+$	372.9
430.9	$[M_2(C_8H_5O_6)(CH_3COO)_2]^+$	432.9
452.9	$[M(C_8H_5O_6)(C_8H_6O_6)]^+$	453.9
508.9	$[M_2(C_8H_4O_6)(C_8H_5O_6)]^+$	510.9

[a]For a complete list of species and assignments, see Tables S3 and S4 in the SI for Ni and Co, respectively.

There are some species with even higher m/z present, but with significantly lower intensity, which we have successfully identified as species up to $\{M_4(H_xdhtp)_3\}$ and $\{M_5(H_xdhtp)_4\}$. This can be evidence of larger species being present in the solution.[47]

When the results for Ni and Co are compared, it is evident that species coming from $Co(OAc)_2{\cdot}4H_2O$ are of higher relative intensity in comparison to those coming from $Ni(OAc)_2{\cdot}4H_2O$. This can be either because $Co(OAc)_2{\cdot}4H_2O$ is easier to ionize in comparison to $Ni(OAc)_2{\cdot}4H_2O$, or that it takes longer for species between H_xdhtp and Co(II) to form than with Ni(II). However, previous reports (and our own observations from the in situ powder X-ray diffraction experiments) indicate that CPO-27-Co forms more quickly than CPO-27-Ni.[42,48] Comprehensive lists of species observed and the assignments are given in Tables S3 and S4 in the SI for Ni and Co, respectively.

Complementary high-resolution ESI-MS spectra were recorded, and the same $\{Ni(H_xdhtp)\}$ species (albeit in hydrated form) are found. Additionally, species assigned to complexes of Ni, acetate, and solvent adducts are present (see Figure S11 and Table S9 in the SI). The lower intensity species have been assigned to solvated $\{Ni_2(H_xdhtp)\}$ and $\{Ni_2(H_xdhtp)_2\}$ and at yet lower intensity to $\{Ni_3(H_xdhtp)_2\}$, all with solvent and/or acetate adducts. Some larger complexes such as $\{Ni_5(H_xdhtp)_4\}$ have been identified in the high-resolution data, but these are of *very* low intensity. See Table S11 in the SI for the corresponding Co results. To summarize, species assigned to $\{M(H_xdhtp)\}$ are the most dominant species as soon as the reactants are mixed, followed by $\{M_2(H_xdhtp)\}$ species and larger species (of reduced intensity) up to $\{M_5(H_xdhtp)_4\}$ complexes, with solvent and/or acetate adducts.

Investigations into the Reactions at 110 °C. At 110 °C, both 1:1 and 2:1 molar ratios of the reactants lead to formation of CPO-27-Ni and -Co, and both of these reactions were investigated. Parallel reactions were set up from the same stock solutions. For Ni, the reactions were stopped at different time intervals and MS measurements were recorded. Aliquots were taken from a few minutes at 110 °C and up to 24 h, when product formation was complete. Product formation typically started after about 2 h at 110 °C. The Co reactions were only investigated by ESI-MS after about 1 day at 110 °C for comparison to the Ni reactions.

We observe definite changes as the reactants are mixed, but as the reaction continues at 110 °C there is little to no change to be observed by ESI-MS. The intensity of species containing both metal and H_xdhtp is typically reduced after 24 h at 110 °C, as one would expect for product formation leading to a decrease in concentration of the species in solution. Some new features have been observed, but these are of *very* low intensity, i.e. do not play a major role, and difficult to assign. In one 1:1 Co reaction m/z 963.8, assigned to $[Co_3(C_8H_4O_6)(C_8H_5O_6)_3]^+$, seems to appear after 24 h at 110 °C; however, this species also appears in some initial measurements at very low intensity, where it does not change in intensity as the reaction proceeds at 110 °C. Therefore, we do not believe this species is playing a major role in the formation of CPO-27-Co. The in-house mass spectra and tables of assignments are shown in Figures S7–S11 and Tables S5–S8, and the complementary high-resolution data for the 1:1 Ni reactions, and the 1:1 and 2:1 Co reactions are shown in section S3 in the SI. There are differences in the solvation stages of the same species observed between the two different instruments used, but the results from both instruments show the mono- and binuclear species $\{M(H_xdhtp)\}$ and $\{M_2(H_xdhtp)\}$ as the most abundant of the metal species assigned to contain H_xdhtp. For the Co reactions, species assigned to $\{M_2(H_xdhtp)\}$ are sometimes almost equal in intensity to species assigned to $\{M(H_xdhtp)\}$. The fact that the ESI-MS spectra remain essentially unchanged over time upon heating strongly indicate that the mono- and dinuclear species $\{M(H_xdhtp)\}$ and $\{M_2(H_xdhtp)\}$ are the key molecular building units in the synthesis of CPO-27-Ni and -Co.

Tandem mass spectrometry (MS/MS) was employed in an attempt to confirm the assignments of the different species reported herein. The results together with experimental results from the mixture of H_4dhtp and $MCl_2{\cdot}6H_2O$ successfully confirmed the assignments of m/z 236.9/237.9, 254.9/255.9 to be $[M(C_8H_3O_5)]^+$ and $[M(C_8H_5O_6)]^+$ (see section S4 in the SI).

Investigations at Room Temperature by ESI-MS. We also investigated the behavior of the same reaction mixtures at room temperature over a minimum of a 2 week period by in-house ESI-MS. We again observe clear changes immediately after the reactants are mixed, and then as the reaction proceeds the ESI-MS spectra remain almost the same, even while the solid product is forming (see section S5 in the SI). Analysis of the microcrystalline materials formed in the 2:1 Ni reactions, and in the 1:1 Ni and Co reactions, were found to be a structure of 1D chains based on $[(M(H_2dhtp)(H_2O)_4){\cdot}2H_2O]$ (see bottom of Figure 1). Additional information is available in

DOI: 10.1021/acs.cgd.8b01657
Cryst. Growth Des. 2019, 19, 2089–2096

section S7 in the SI. The same chain structure, but with DMSO and H_2O as solvate molecules, has been reported previously.[49]

The 2:1 Co reactions resulted in larger needle-shaped pink crystals. The compound was confirmed by PXRD analysis to be solvated CPO-27-Co (see comparison in Figure S20 in SI). This highlights a significant difference in the behavior of the nickel and cobalt cations, which was unexpected considering how similar the two metals have behaved otherwise. Osta et al. compared the synthesis of CPO-27-Ni and -Co in 2013,[42] where they concluded that the Co material crystallizes more rapidly than the Ni analogue, and perhaps this might be one of the reasons we see this difference in behavior. The yields of the 1:1 reactions are around 50% for both cobalt and nickel, while the 2:1 reactions result in yields as low as 10% for both. Larger yields can be obtained, but typically with H_4dhtp impurities.

Importantly, despite these reactions resulting in different crystalline products, the ESI-MS analysis shows close to identical species in solution for the initial mixture and while the product forms, with the previously identified $\{M(H_xdhtp)\}$ and $\{M_2(H_xdhtp)\}$ species being the key species present in solution. It is straightforward to anticipate that the key species in solution contribute most to the crystal growth as they are incorporated into the product. In this case, it means the same species, the mononuclear species $\{M(H_xdhtp)\}$ and, possibly to a lesser extent, the dinuclear species $\{M_2(H_xdhtp)\}$, play the key role in the crystal growth of both the CPO-27 structure with its condensed metal−oxygen polyhedra and the 1D network $[M(H_2dhtp)(H_2O)_4]$ with isolated metal cations. Larger intermediate species are not observed as major solutes in the ESI-MS, which we interpret to mean that nucleation and crystal growth from the mono- and dinuclear species apparently occur so rapidly that larger species play no significant role in the crystal growth.

Synchrotron Investigations. An in situ, time-resolved powder diffraction study of the formation of CPO-27-Ni was carried out. A 2:1 molar ratio reaction of $Ni(OAc)_2{\cdot}4H_2O$ and H_4dhtp in 1:1 (v:v) H_2O and THF was prepared in a sealed capillary (0.5 mm) and inserted into the X-ray beam. A heat gun was employed to heat the reaction mixture from room temperature to 110 °C with 5 °C min^{-1}, with X-ray data being collected simultaneously. There were no diffraction peaks to be observed at time 0 (scan 1), meaning there is nothing crystalline present in the reaction mixture at this stage. There are no diffraction peaks present before we reach 110 °C (scan no. 12), at which point we observe a rapid increase in the intensity of the (110) and (030) reflections, as can be seen in Figure 4. These two reflections are typical for the CPO-27-Ni structure. In accordance with previously reported results, we can confirm that for the CPO-27-Ni structure there is no intermediate crystalline species forming in the reaction solution between $Ni(OAc)_2{\cdot}4H_2O$ and H_4dhtp. This is in agreement with recent time-resolved PXRD results, which showed that the crystallite formation of ZIF-8 is already complete after 8 s of reaction time.[50] As the reaction continues, the complete PXRD pattern expected for hydrated CPO-27-Ni is clearly observed.

The full width at half-maximum (FWHM) of the first two reflection peaks decreases quickly (see section S8 in SI) as the initially formed crystallites start growing as soon as the concentration of reactants in the reaction mixture has decreased below the level leading to the initial nucleation. Similar observations have been reported by Osta et al., where

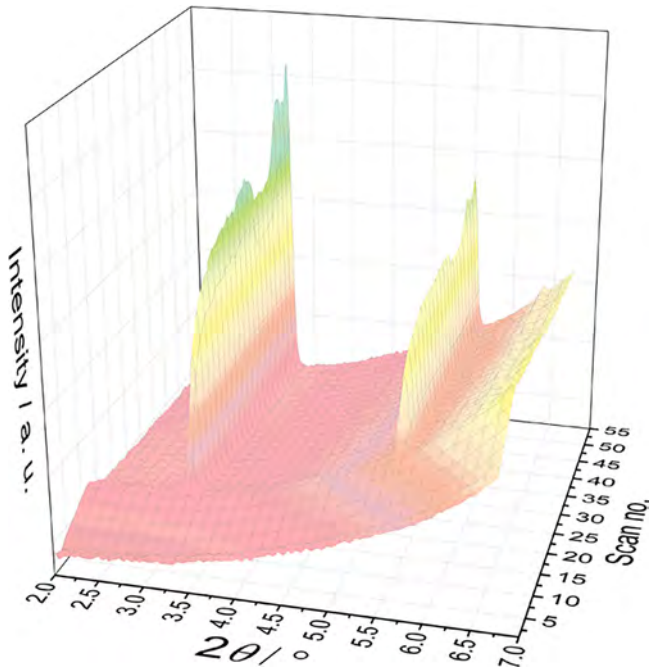

Figure 4. Synchrotron PXRD data, showing the formation of CPO-27-Ni in a capillary reactor experiment. The observed dip in intensity occurs because the suspension is no longer homogeneous (the crystals become larger and start to move around inside the capillary, resulting in variation in the amount being irradiated by the beam).

they observed a longer nucleation time for Ni in comparison with Co.[42] This was also consistent with previous reports by Haque et al.,[48] where they proposed that the difference was due to the higher lability of $[Co(H_2O)_6]^{2+}$, which is responsible for the enhanced rate of reaction with the carboxylate ligand via increased solvent−ligand exchange kinetics.

DISCUSSION

The time-resolved powder diffraction study confirms that the first crystalline product observed is CPO-27-M (M = Co, Ni), as evidenced by the two strong diffraction peaks appearing a few minutes after the reaction mixture reached a temperature of 110 °C. The crystallization at room temperature resulted in a 1D chain structure from the 2:1 and 1:1 molar ratio Ni reactions and 1:1 molar ratio Co reactions, while the 2:1 molar ratio Co reactions result in the CPO-27-Co structure. Clear changes were observed by ESI-MS when the reactants were mixed, and then as the reactions proceeded at room temperature little to no change was observed, not even when a precipitate started forming. Finally, the MS spectra of the 110 °C reactions were also very similar to those observed for the reactions at room temperature. We conclude on the basis of these observations that the species present in the reaction mixture do not change significantly as the crystallization proceeds and the solid product is formed. These species also represent the building blocks from which the metal−organic framework is constructed.

From the extensive ESI-MS analyses carried out herein, we know that the spectra change significantly as soon as the reactants are mixed. In the spectra, the $\{M(H_xdhtp)\}$ species are most evident, followed by the $\{M_2(H_xdhtp)_2\}$ species, as well as metal complexes containing only acetate and/or solvent molecules. Because we observe these $\{M(H_xdhtp)\}$ and

DOI: 10.1021/acs.cgd.8b01657
Cryst. Growth Des. 2019, 19, 2089−2096

$\{M_2(H_xdhtp)_2\}$ species so clearly with significant intensity in the spectra from both ESI-MS instruments, these species are likely the key building blocks in the formation of CPO-27-M, as well as for the 1D $[(M(H_2dhtp)(H_2O)_4)\cdot 2H_2O]$ structure. The metal to H_xdhtp ratio in the final CPO-27-M structure is 2:1; thus, in addition to the $\{M(H_xdhtp)\}$ and $\{M_2(H_xdhtp)\}$ species, metal complexes of M_1 with solvent and/or acetate adducts, which are always present in the ESI-MS analysis, must also be involved in the crystallization process.

Larger, more complex species were observed by ESI-MS, but at very low intensities. Either these species are products of the ionization or larger species are also present in the reaction mixture. However, if there were significant amounts of larger species (up to m/z 2500) present in the solution, they would be expected to be visible with significant intensity in the spectra recorded using the high-resolution ESI-MS. As this is not the case, we conclude that the initial solid nuclei that are too heavy to be observable using the ESI-MS technique (i.e., cannot be sufficiently ionized into the gas phase) have assembled rapidly from the smaller species present in solution. Further crystal growth then occurs by addition of smaller species to the present nuclei and crystallites. We propose that these smaller $\{M(H_xdhtp)\}$ and $\{M_2(H_xdhtp)\}$ species together with M_1 solvent and/or acetate complexes are the key building blocks for the final crystalline compound. In any of these, one metal center coordinates a maximum of two H_xdhtp units, and it is interesting to note that the same species are typically observed independent of the final product being CPO-27-M or $[(M(H_2dhtp)(H_2O)_4)\cdot 2H_2O]$, which is a strong argument for smaller species being a key part of the formation of both materials. Serre et al. have reported an X-ray study where they identified discrete, fully formed secondary building units (SBUs) present prior to the formation of the MOF known as MIL-89.[51] Henderson et al. also found that ESI-MS as a technique is useful in the identification of stable SBUs prior to crystal growth.[13,19] It is not possible to identify such SBUs for the CPO-27 structure due to the nature of the infinite chain structure, which also can explain why we do not observe larger species during the formation of CPO-27-M.

CONCLUSIONS

A better understanding of the elusive self-assembly processes can contribute to address the challenge of preparing new, robust MOFs with desired properties for specific applications. A part of this understanding is improved insight into the species present under reaction conditions and reactions occurring in the solution on the molecular level.

Here, we have performed an investigation into the formation of CPO-27-Ni and -Co utilizing electrospray ionization mass spectrometry (ESI-MS). Time-resolved PXRD analyses do not show any intermediary crystalline species except CPO-27-M (M = Co, Ni) during the reaction, and the product formation starts within minutes when the reaction is kept at 110 °C. When the reaction is followed using ESI-MS, clear changes were observed in the spectra as the reactants were mixed, but as the reaction continued, the spectra remained very similar. The fact that there was hardly any development of species observed by ESI-MS over time as the reactions proceeded was unexpected and indicates that the species in solution are more rapidly incorporated into the growing crystallite rather than forming species with multiple cations in solution. We have identified the mono- and dinuclear species $\{M(H_xdhtp)\}$ and $\{M_2(H_xdhtp)\}$ as key linker-containing building blocks in the formation of CPO-27-M, as well as in the formation of the 1D chain structure $[(M(H_2dhtp)(H_2O)_4\cdot 2H_2O]$ obtained from room-temperature reactions.

ASSOCIATED CONTENT

Supporting Information

The Supporting Information is available free of charge on the ACS Publications website at DOI: 10.1021/acs.cgd.8b01657.

Further details on ESI-MS experiments and assignments, along with crystallographic details (PDF)

Accession Codes

CCDC 1499898 contains the supplementary crystallographic data for this paper. These data can be obtained free of charge via www.ccdc.cam.ac.uk/data_request/cif, or by emailing data_request@ccdc.cam.ac.uk, or by contacting The Cambridge Crystallographic Data Centre, 12 Union Road, Cambridge CB2 1EZ, UK; fax: +44 1223 336033.

AUTHOR INFORMATION

Corresponding Authors

*E-mail for M.H.R.: mali.rosnes@uib.no.
*E-mail for P.D.C.D.: Pascal.Dietzel@uib.no.

ORCID

Mali H. Rosnes: 0000-0003-3274-9967
Karl W. Törnroos: 0000-0001-6140-5915
Rune E. Johnsen: 0000-0002-9929-6942
Leroy Cronin: 0000-0001-8035-5757
Pascal D. C. Dietzel: 0000-0001-5731-2118

Notes

The authors declare no competing financial interest.

ACKNOWLEDGMENTS

The authors thank Dr. Bjarte Holmelid and acknowledge the support from the Research Council of Norway through the FRINATEK program (grant 221596). We also want to thank the staff at the Swiss-Norwegian Beamlines at ESRF.

REFERENCES

(1) Saha, R.; Joarder, B.; Roy, A. S.; Manirul Islam, S.; Kumar, S. Simultaneous Presence of Both Open Metal Sites and Free Functional Organic Sites in a Noncentrosymmetric Dynamic Metal−Organic Framework with Bimodal Catalytic and Sensing Activities. *Chem. - Eur. J.* **2013**, *19*, 16607−16614.

(2) Xamena, F. L. i.; Gascon, J. *Metal Organic Frameworks as Heterogeneous Catalysts*; Royal Society of Chemistry: Cambridge, U.K., 2013.

(3) Yu, D.; Yazaydin, A. O.; Lane, J. R.; Dietzel, P. D. C.; Snurr, R. Q. A combined experimental and quantum chemical study of CO2 adsorption in the metal-organic framework CPO-27 with different metals. *Chem. Sci.* **2013**, *4*, 3544−3556.

(4) Mathieson, J. S.; Cooper, G. J. T.; Pickering, A. L.; Keller, M.; Long, D.-L.; Newton, G. N.; Cronin, L. Monitoring the Formation of Coordination Complexes Using Electrospray Mass Spectrometry. *Chem. - Asian J.* **2009**, *4*, 681−687.

(5) Mathieson, J. S.; Rosnes, M. H.; Sans, V.; Kitson, P. J.; Cronin, L. Continuous parallel ESI-MS analysis of reactions carried out in a bespoke 3D printed device. *Beilstein J. Nanotechnol.* **2013**, *4*, 285−291.

(6) Hirsch, K. A.; Wilson, S. R.; Moore, J. S. Association of Dicyanodiphenylacetylenes with Silver(I) Salts in Solution and Solid State: Electrospray Ionization Mass Spectrometry Samples Aggregates at Subsaturated Concentrations. *J. Am. Chem. Soc.* **1997**, *119*, 10401−10412.

DOI: 10.1021/acs.cgd.8b01657
Cryst. Growth Des. 2019, 19, 2089−2096

(7) Yang, H.-B.; Northrop, B. H.; Zheng, Y.-R.; Ghosh, K.; Lyndon, M. M.; Muddiman, D. C.; Stang, P. J. Synthesis of Six-Component Metallodendrimers via [3 + 3] Coordination-Driven Self-Assembly. *J. Org. Chem.* **2009**, *74*, 3524−3527.
(8) Wilson, E. F.; Miras, H. N.; Rosnes, M. H.; Cronin, L. Real-Time Observation of the Self-Assembly of Hybrid Polyoxometalates Using Mass Spectrometry. *Angew. Chem., Int. Ed.* **2011**, *50*, 3720−3724.
(9) Rosnes, M. H.; Musumeci, C.; Pradeep, C. P.; Mathieson, J. S.; Long, D.-L.; Song, Y.-F.; Pignataro, B.; Cogdell, R.; Cronin, L. Assembly of Modular Asymmetric Organic−Inorganic Polyoxometalate Hybrids into Anisotropic Nanostructures. *J. Am. Chem. Soc.* **2010**, *132*, 15490−15492.
(10) Wilson, E. F.; Abbas, H.; Duncombe, B. J.; Streb, C.; Long, D.-L.; Cronin, L. Probing the Self-Assembly of Inorganic Cluster Architectures in Solution with Cryospray Mass Spectrometry: Growth of Polyoxomolybdate Clusters and Polymers Mediated by Silver(I) Ions. *J. Am. Chem. Soc.* **2008**, *130*, 13876−13884.
(11) Seeber, G.; Cooper, G. J. T.; Newton, G. N.; Rosnes, M. H.; Long, D.-L.; Kariuki, B. M.; Kogerler, P.; Cronin, L. Following the self assembly of supramolecular MOFs using X-ray crystallography and cryospray mass spectrometry. *Chem. Sci.* **2010**, *1*, 62−67.
(12) Garibay, S. J.; Wang, Z.; Tanabe, K. K.; Cohen, S. M. Postsynthetic Modification: A Versatile Approach Toward Multifunctional Metal-Organic Frameworks. *Inorg. Chem.* **2009**, *48*, 7341−7349.
(13) Rood, J. A.; Boggess, W. C.; Noll, B. C.; Henderson, K. W. Assembly of a Homochiral, Body-Centered Cubic Network Composed of Vertex-Shared Mg12 Cages: Use of Electrospray Ionization Mass Spectrometry to Monitor Metal Carboxylate Nucleation. *J. Am. Chem. Soc.* **2007**, *129*, 13675−13682.
(14) Lim, I. H.; Schrader, W.; Schüth, F. Insights into the Molecular Assembly of Zeolitic Imidazolate Frameworks by ESI-MS. *Chem. Mater.* **2015**, *27*, 3088−3095.
(15) Lim, I. H.; Schrader, W.; Schüth, F. The formation of zeolites from solution − Analysis by mass spectrometry. *Microporous Mesoporous Mater.* **2013**, *166*, 20−36.
(16) Wagia, R.; Strashnov, I.; Anderson, M. W.; Attfield, M. P. Determination of the Preassembled Nucleating Units That Are Critical for the Crystal Growth of the Metal−Organic Framework CdIF-4. *Angew. Chem., Int. Ed.* **2016**, *55*, 9075−9079.
(17) Terban, M. W.; Banerjee, D.; Ghose, S.; Medasani, B.; Shukla, A.; Legg, B. A.; Zhou, Y.; Zhu, Z.; Sushko, M. L.; De Yoreo, J. J.; Liu, J.; Thallapally, P. K.; Billinge, S. J. L. Early stage structural development of prototypical zeolitic imidazolate framework (ZIF) in solution. *Nanoscale* **2018**, *10*, 4291−4300.
(18) Rosnes, M. H.; Nesse, F. S.; Opitz, M.; Dietzel, P. D. C. Morphology control in modulated synthesis of metal-organic framework CPO-27. *Microporous Mesoporous Mater.* **2019**, *275*, 207−213.
(19) Rood, J. A. *Metal-Organic Frameworks as Functional, Porous Materials*; University of Notre Dame: Notre Dame, IN, 2009.
(20) Dietzel, P. D. C.; Morita, Y.; Blom, R.; Fjellvåg, H. An In Situ High-Temperature Single-Crystal Investigation of a Dehydrated Metal−Organic Framework Compound and Field-Induced Magnetization of One-Dimensional Metal−Oxygen Chains. *Angew. Chem., Int. Ed.* **2005**, *44*, 6354−6358.
(21) Dietzel, P. D. C.; Panella, B.; Hirscher, M.; Blom, R.; Fjellvåg, H. Hydrogen adsorption in a nickel based coordination polymer with open metal sites in the cylindrical cavities of the desolvated framework. *Chem. Commun.* **2006**, 959−961.
(22) Dietzel, P. D. C.; Blom, R.; Fjellvåg, H. Base-Induced Formation of Two Magnesium Metal-Organic Framework Compounds with a Bifunctional Tetratopic Ligand. *Eur. J. Inorg. Chem.* **2008**, *2008*, 3624−3632.
(23) Zhou, W.; Wu, H.; Yildirim, T. Enhanced H2 Adsorption in Isostructural Metal−Organic Frameworks with Open Metal Sites: Strong Dependence of the Binding Strength on Metal Ions. *J. Am. Chem. Soc.* **2008**, *130*, 15268−15269.
(24) Rosi, N. L.; Kim, J.; Eddaoudi, M.; Chen, B.; O'Keeffe, M.; Yaghi, O. M. Rod Packings and Metal−Organic Frameworks Constructed from Rod-Shaped Secondary Building Units. *J. Am. Chem. Soc.* **2005**, *127*, 1504−1518.
(25) Bloch, E. D.; Murray, L. J.; Queen, W. L.; Chavan, S.; Maximoff, S. N.; Bigi, J. P.; Krishna, R.; Peterson, V. K.; Grandjean, F.; Long, G. J.; Smit, B.; Bordiga, S.; Brown, C. M.; Long, J. R. Selective Binding of O2 over N2 in a Redox−Active Metal−Organic Framework with Open Iron(II) Coordination Sites. *J. Am. Chem. Soc.* **2011**, *133*, 14814−14822.
(26) Märcz, M.; Johnsen, R. E.; Dietzel, P. D. C.; Fjellvåg, H. The iron member of the CPO-27 coordination polymer series: Synthesis, characterization, and intriguing redox properties. *Microporous Mesoporous Mater.* **2012**, *157*, 62−74.
(27) Calleja, G.; Sanz, R.; Orcajo, G.; Briones, D.; Leo, P.; Martínez, F. Copper-based MOF-74 material as effective acid catalyst in Friedel−Crafts acylation of anisole. *Catal. Today* **2014**, *227*, 130−137.
(28) Sanz, R.; Martínez, F.; Orcajo, G.; Wojtas, L.; Briones, D. Synthesis of a honeycomb-like Cu-based metal-organic framework and its carbon dioxide adsorption behaviour. *Dalton Trans.* **2013**, *42*, 2392−2398.
(29) Rosnes, M. H.; Opitz, M.; Frontzek, M.; Lohstroh, W.; Embs, J. P.; Georgiev, P. A.; Dietzel, P. D. C. Intriguing differences in hydrogen adsorption in CPO-27 materials induced by metal substitution. *J. Mater. Chem. A* **2015**, *3*, 4827−4839.
(30) Díaz-García, M.; Sánchez-Sánchez, M. Synthesis and characterization of a new Cd-based metal-organic framework isostructural with MOF-74/CPO-27 materials. *Microporous Mesoporous Mater.* **2014**, *190*, 248−254.
(31) Valvekens, P.; Vandichel, M.; Waroquier, M.; Van Speybroeck, V.; De Vos, D. Metal-dioxidoterephthalate MOFs of the MOF-74 type: Microporous basic catalysts with well-defined active sites. *J. Catal.* **2014**, *317*, 1−10.
(32) Dietzel, P. D. C.; Besikiotis, V.; Blom, R. Application of metal-organic frameworks with coordinatively unsaturated metal sites in storage and separation of methane and carbon dioxide. *J. Mater. Chem.* **2009**, *19*, 7362−7370.
(33) Caskey, S. R.; Wong-Foy, A. G.; Matzger, A. J. Dramatic Tuning of Carbon Dioxide Uptake via Metal Substitution in a Coordination Polymer with Cylindrical Pores. *J. Am. Chem. Soc.* **2008**, *130*, 10870−10871.
(34) Dietzel, P. D. C.; Johnsen, R. E.; Fjellvåg, H.; Bordiga, S.; Groppo, E.; Chavan, S.; Blom, R. Adsorption properties and structure of CO2 adsorbed on open coordination sites of metal-organic framework Ni2(dhtp) from gas adsorption, IR spectroscopy and X-ray diffraction. *Chem. Commun.* **2008**, 5125−5127.
(35) Burtch, N. C.; Jasuja, H.; Walton, K. S. Water Stability and Adsorption in Metal−Organic Frameworks. *Chem. Rev.* **2014**, *114*, 10575−10612.
(36) Ramanan, A.; Whittingham, M. S. How Molecules Turn into Solids: the Case of Self-Assembled Metal−Organic Frameworks. *Cryst. Growth Des.* **2006**, *6*, 2419−2421.
(37) Stock, N.; Reinsch, H.; Schillinger, L.-H., Synthesis of MOFs. In *Metal Organic Frameworks as Heterogenous Catalysts*; Xamena, F. X. L. i.; Gascon, J., Eds.; Henry Ling: Dorchester, U.K., 2013.
(38) Guasch, J.; Dietzel, P. D. C.; Collier, P.; Acerbi, N. The effect of solvent and temperature in the synthesis of CPO-27-Ni by reflux. *Microporous Mesoporous Mater.* **2015**, *203*, 238−244.
(39) Garzon-Tovar, L.; Carne-Sanchez, A.; Carbonell, C.; Imaz, I.; Maspoch, D. Optimised room temperature, water-based synthesis of CPO-27-M metal-organic frameworks with high space-time yields. *J. Mater. Chem. A* **2015**, *3*, 20819−20826.
(40) Stavitski, E.; Goesten, M.; Juan-Alcañiz, J.; Martiñez-Joaristi, A.; Serra-Crespo, P.; Petukhov, A. V.; Gascon, J.; Kapteijn, F. Kinetic Control of Metal−Organic Framework Crystallization Investigated by Time-Resolved In Situ X-Ray Scattering. *Angew. Chem., Int. Ed.* **2011**, *50*, 9624−9628.
(41) Millange, F.; Medina, M. I.; Guillou, N.; Férey, G.; Golden, K. M.; Walton, R. I. Time-Resolved In Situ Diffraction Study of the

DOI: 10.1021/acs.cgd.8b01657
Cryst. Growth Des. 2019, 19, 2089−2096

Solvothermal Crystallization of Some Prototypical Metal−Organic Frameworks. *Angew. Chem., Int. Ed.* **2010**, *49*, 763−766.
(42) El Osta, R. E.; Feyand, M.; Stock, N.; Millange, F.; Walton, R. I. Crystallisation Kinetics of Metal Organic Frameworks From in situ Time-Resolved X-ray Diffraction. *Powder Diffr.* **2013**, *28*, S256−S275.
(43) Yeung, H. H. M.; Wu, Y.; Henke, S.; Cheetham, A. K.; O'Hare, D.; Walton, R. I. In Situ Observation of Successive Crystallizations and Metastable Intermediates in the Formation of Metal−Organic Frameworks. *Angew. Chem., Int. Ed.* **2016**, *55*, 2012−2016.
(44) Wu, Y.; Moorhouse, S. J.; O'Hare, D. Time-Resolved in Situ Diffraction Reveals a Solid-State Rearrangement During Solvothermal MOF Synthesis. *Chem. Mater.* **2015**, *27*, 7236−7239.
(45) Jolivet, J.-P. *Metal Oxide Chemistry and Synthesis - From Solution to Solid State*; Wiley: Chichester, U.K., 2000.
(46) Hammersley, A. P.; Svensson, S. O.; Hanfland, M.; Fitch, A. N.; Hausermann, D. Two-dimensional detector software: From real detector to idealised image or two-theta scan. *High Pressure Res.* **1996**, *14*, 235−248.
(47) McDonald, L. W.; Campbell, J. A.; Clark, S. B. Failure of ESI Spectra to Represent Metal-Complex Solution Composition: A Study of Lanthanide−Carboxylate Complexes. *Anal. Chem.* **2014**, *86*, 1023−1029.
(48) Haque, E.; Jhung, S. H. Synthesis of isostructural metal−organic frameworks, CPO-27s, with ultrasound, microwave, and conventional heating: Effect of synthesis methods and metal ions. *Chem. Eng. J.* **2011**, *173*, 866−872.
(49) Rosa, I. M. L.; Costa, M. C. S.; Vitto, B. S.; Amorim, L.; Correa, C. C.; Pinheiro, C. B.; Doriguetto, A. C. Influence of Synthetic Methods in the Structure and Dimensionality of Coordination Polymers. *Cryst. Growth Des.* **2016**, *16*, 1606−1616.
(50) Polyzoidis, A.; Etter, M.; Herrmann, M.; Loebbecke, S.; Dinnebier, R. E. Revealing the Initial Reaction Behavior in the Continuous Synthesis of Metal−Organic Frameworks Using Real-Time Synchrotron X-ray Analysis. *Inorg. Chem.* **2017**, *56*, 5489−5492.
(51) Surble, S.; Millange, F.; Serre, C.; Ferey, G.; Walton, R. I. An EXAFS study of the formation of a nanoporous metal-organic framework: evidence for the retention of secondary building units during synthesis. *Chem. Commun.* **2006**, 1518−1520.

DOI: 10.1021/acs.cgd.8b01657
Cryst. Growth Des. 2019, 19, 2089−2096